A Reconfigurable Two-stage 11kW DC-DC Resonant Converter for EV Charging with a 150-1000V Output Voltage Range

Aarninkhof, Bram Oude; Lyu, Dingsihao; Soeiro, Thiago Batista; Bauer, Pavol

DOI
10.1109/tte.2023.3279211

Publication date
2023

Document Version
Final published version

Published in
IEEE Transactions on Transportation Electrification

A Reconfigurable Two-Stage 11 kW DC–DC Resonant Converter for EV Charging With a 150–1000 V Output Voltage Range

Bram Oude Aarninkhof, Dingsihao Lyu, *Member, IEEE*, Thiago Batista Soeiro, *Senior Member, IEEE*, and Pavol Bauer, *Senior Member, IEEE*

***Abstract*— In this article, a reconfigurable two-stage dc/dc resonant topology with a wide output voltage range of 150–1000 V is proposed for electric vehicle (EV) charging with high efficiency over the entire load range. The proposed topology consists of an LLC resonant converter with dual secondary sides; two interleaved triangular current mode (TCM) buck converters, and three additional auxiliary switches for reconfiguration. Two possible arrangements of the proposed topology are considered and compared. The analytical model of the topology is developed, which is used for the efficiency estimation of different configurations and the design of the prototype converter. An 11 kW hardware demonstrator is built and tested. The maximum measured efficiency of the converter is 97.66%, with a >95% efficiency over the complete 150–1000 V range at full power. The proposed two-stage converter achieves the widest output voltage range reported in literature for resonant power converters (RPCs), thereby capable of charging existing and future EVs very efficiently over any charging cycle.**

***Index Terms*— DC–DC converters, electric vehicle (EV), EV charger, LLC, resonant converter, triangular current mode (TCM) buck, wide output voltage range.**

I. Introduction

THE electrification of the world's transportation fleet has gained momentum in recent years. For example the widespread use of electric vehicles (EVs) today. This shift to EVs is all in light of a global effort to reduce global greenhouse gas (GHG) emissions [1]. Consequently, the demand for public EV chargers to accommodate all these vehicles will increase correspondingly. According to the sustainable development scenario (SDS) [2], 6% of the electricity consumption in the European Union in 2030 will come from EV charging, compared to 0.2% in 2019.

Most EVs currently produced use a battery pack with a nominal voltage of 400 V. However, in recent years, some models have been announced that use a higher voltage battery architecture [3]. This higher battery voltage which is typically close to 800 V can be one of the solutions enabling a faster charging time of EVs [25].

The introduction of these higher voltage battery architectures imposes a challenge on the EV chargers: the (common) 400 V battery architecture as well as the new high voltage battery architectures need to be accommodated. As a result, the typical dc/dc converters used in the EV chargers must operate in an extremely wide output voltage range.

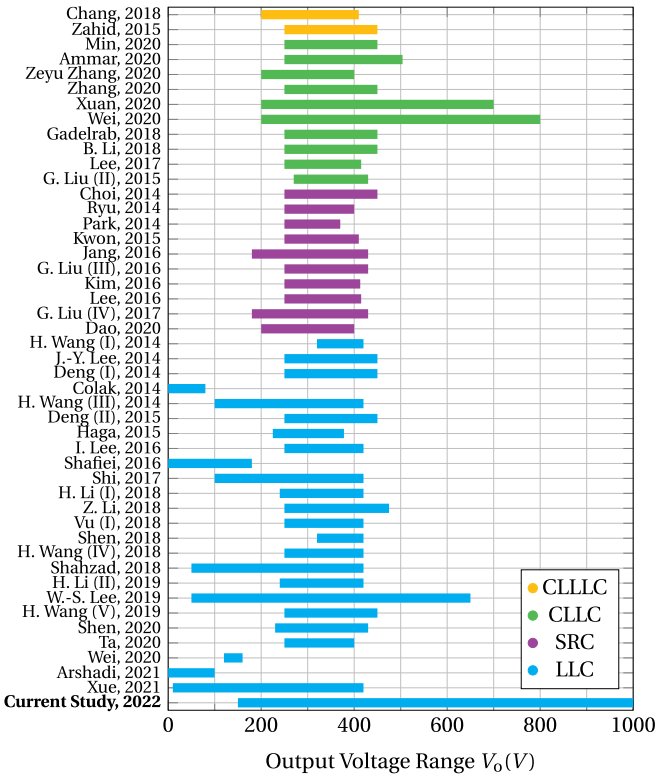

Fig. 1. Overview of the output voltage range of all studies found regarding RPCs and EV charging from 2014 to 2022 [5], [6], [7], [8], [9], [10], [11], [13], [14], [27], [28], [29], [30], [31], [32], [33], [34], [35], [36], [37], [38], [39], [40], [41], [42], [43], [44], [45], [46], [47], [48], [49], [50], [51], [52], [53], [54], [55], [56], [57], [58], [59], [60], [61].

Manuscript received 19 November 2022; revised 6 March 2023 and 1 May 2023; accepted 12 May 2023. Date of publication 23 May 2023; date of current version 16 March 2024. This work was supported in part by the European H2020 Research and Innovation Program; in part by the ECSEL Joint Undertaking; and in part by the National Funding Authorities from eight participating countries, such as Austria, Finland, Germany, including the Free States of Saxony and Thuringia, Hungary, The Netherlands, Slovakia, Spain, and Switzerland, under Grant 826417. *(Corresponding author: Dingsihao Lyu.)*

Bram Oude Aarninkhof and Thiago Batista Soeiro are with the Faculty of Electrical Engineering, Mathematics and Computer Science (EEMCS), University of Twente, 7522 NB Enschede, The Netherlands (e-mail: b.j.oudeaarninkhof@utwente.nl; t.batistasoeiro@utwente.nl).

Dingsihao Lyu and Pavol Bauer are with the Faculty of Electrical Engineering, Mathematics and Computer Science (EEMCS), Delft University of Technology (TU Delft), 2628 CD Delft, The Netherlands (e-mail: d.lyu@tudelft.nl; p.bauer@tudelft.nl).

Digital Object Identifier 10.1109/TTE.2023.3279211

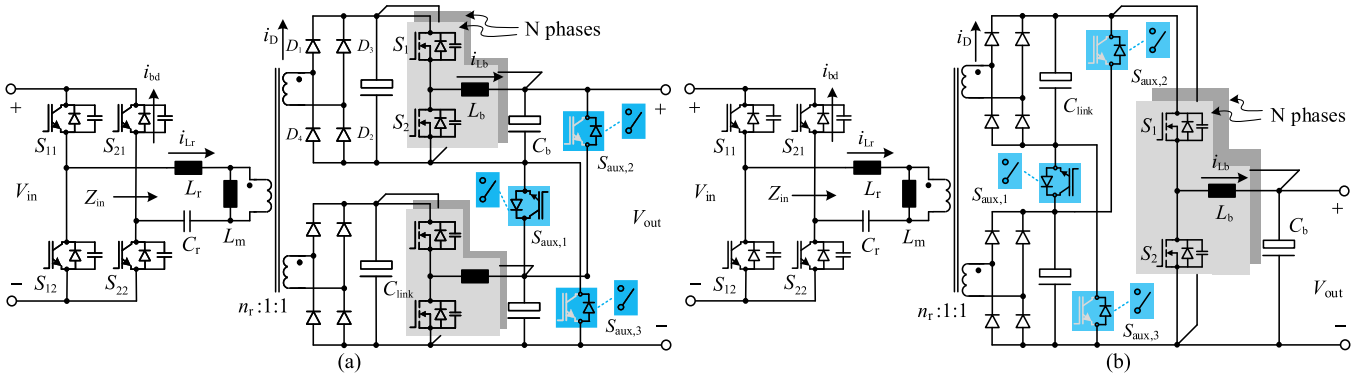

Fig. 2. Schematics of the proposed reconfigurable two-stage RPC in two different arrangements. Note that $S_{\text{aux},1/2/3}$ can be either mechanical switches or semiconductor transistors. (a) Configuration I: S_{aux} after the interleaved BUCK stage (selected). (b) Configuration II: S_{aux} before the interleaved BUCK stage.

However, few studies in literature have provided experimentally verified isolated dc/dc converter designs that are able to charge both the 400 and 800 V EVs, though Lyu et al. [15] proposed a reconfigurable phase shifted full bridge (PSFB) to achieve this wide output voltage range. For resonant power converters (RPC), no such large output voltage range has been achieved [5], [6], [7], [8], [9], [10], [11], [13], [14], [27], [28], [29], [30], [31], [32], [33], [34], [35], [36], [37], [38], [39], [40], [41], [42], [43], [44], [45], [46], [47], [48], [49], [50], [51], [52], [53], [54], [55], [56], [57], [58], [59], [60], [61]. Based on the studies about the resonant converters in the EV charging application in the past decade (2010–2021), Fig. 1 shows the reported output voltage ranges of the RPCs. Most of the studies report an output voltage range between 250 and 450 V, corresponding with the typical battery voltage of a 400 V battery architecture. Seven studies reported an output voltage range of $\Delta V_o > 320$ V [5], [6], [7], [8], [9], [10], [11].

The challenge lies in the poor efficiency performance when these converters are made to operate in such a wide voltage range. The RPC is typically controlled by frequency modulation, and it is well-known for its high-efficiency performance when it is operated at the resonant frequency point. However, operating the RPCs with frequency modulation in a wide output voltage range will result in a wide switching frequency range, which brings the issues of more complicated magnetic component design, a decrease in efficiency, and reduced EMI performance [12]. As a result, the conventional RPC, such as an LLC converter, is not able to provide high efficiency in a wide voltage range application.

To extend the output voltage conversion range of the RPCs without compromising the system efficiency performance in the whole operational range, mainly five methods can be found in the literature. The first method uses a variable input dc link voltage while operating the RPC in the resonant frequency point [5], [6]. The output voltage regulation of the RPC using this method is entirely performed by the variable input voltage. The direct benefit of this method is that the RPC is operated at the maximum efficiency point with a simple fixed frequency modulation. However, this method requires a controlled front-end converter which provides the adjustable input dc link voltage for the RPC. As a result, the design and implementation complexity shift from the RPC converter to the front-end converter.

The second method is based on having two RPC converters operating in an interleaving way. Both switch at the resonant switching frequency, and they are phase-shifted to control the output voltage [9]. This method operates the RPCs with a constant switching frequency, which is easy to implement and provides ZVS and high efficiency for the individual RPCs. However, due to the increase of circulating current-induced conduction loss, the interleaved RPC has a significant efficiency drop when the output voltage is low.

The third method uses a three-level bidirectional RPC together with pulse frequency modulation (PFM), often abbreviated as; frequency modulation [8]. This RPC features two pairs of three-level full bridges, a resonant inductor and a capacitor. By combining the four operational modes of each of the three-level full bridges, this three-level bidirectional RPC adapts to a wide output voltage range with a small range of switching frequency change. However, the trade-off is the cost of the converter and control complexity, as it requires a total of 16 transistors.

The fourth method is to use a flexible voltage gain control scheme for the full-bridge resonant converter, for example, proposed by Wei et al. [7]. A flexible voltage gain control could be a combination of reconfiguration between full-bridge and half-bridge of the switching bridge [63], a variable dc-link voltage provided by the grid-connected circuit and/or series compensation capacitance [64], phase shift modulation (PSM) which results in a controllable duty cycle of the H-bridge inverter, and dual control where both frequency modulation and PSM are implemented together [26]. These approaches extend the voltage range by the increased control complexity without modification on the converter topology.

The fifth method uses a two-stage structure, where the RPC is the first stage, followed by a buck converter as the second stage [11]. This two-stage solution allowed for a decoupling of the functions of the proposed converter: the resonant stage provides galvanic isolation and a constant voltage step-up through the turns ratio of the transformer. Only the buck converter controls the output voltage since the LLC is operated only at the resonant frequency. Consequently, this approach achieves a wide voltage regulation range with a simple control scheme due to the control decoupling of the two stages. However, the drawback is higher cost, and the efficiency performance depends on this additional stage.

TABLE I
COMPARISON OF ALL WIDE OUTPUT VOLTAGE RANGE SOLUTIONS INVOLVING AN RPC

	Variable input voltage SEPIC PFC + LLC [5]	Variable input voltage SEPIC PFC + LLC [6]	Two interleaved LLC converters [9]	Three level CLLC Converter [8]	Combination of Control Strategies CLLC converter [7]	Two-Stage: LLC + buck converter [11]
Modulation	Constant f_{sw}, Variable V_{in}	Constant f_{sw}, Variable V_{in}	PSM	PFM + Variable operational modes	PFM + Variable V_{in} + reconfig. HB or FB	LLC: Constant f_{sw} buck: Duty cycle
Output Voltage range	100-420 V	100-420 V	10-420 V	200-700 V	200-800 V	50-650 V
Switching frequency range	-	200 kHz	100 kHz	31-70 kHz	140-250 kHz	120 kHz & 50 kHz
Number of switches	5	5	4	16	8	5
Number of Diodes	9*	9*	4	4	0	9
Number of Transformers	1	1	2	1	1	2
Peak efficiency	97.4%	88.4%	98.10%	96.8%	98.5%	97.32%
Maximum Power	3.3 kW	3.3 kW	1 kW	3.5 kW	22 kW	20 kW
Control Complexity	Moderate	Moderate	Moderate	Complex	Complex	Simple
Power Density	-	-	-	-	8 kW/L	-

A comparison of all studies regarding wide output voltage range RPCs is given in Table I. It can be seen that, in the case of designing an RPC for wide voltage regulation when a bidirectional operation is not a necessity, the two-stage approach is the conventional way to be implemented. The RPC stage can operate at a constant frequency near the series resonant frequency, allowing for the optimal design of the magnetic components and minimal losses. Besides this, ZVS of the primary switches is guaranteed for the entire operating range. However, the efficiency performance of the two-stage solution still has room for improvement. When a simple continuous conduction mode (CCM) buck converter is used for the voltage regulation stage, the efficiency is limited by mainly two factors, namely the turn-on switching loss and the low duty cycle when the output voltage is low. As a result, the two-stage RPC converter will suffer from a considerable efficiency drop during; moments of heavy load where the turn-on switching loss is high, and moments when the output voltage, and thus the equivalent duty cycle, is low.

Commercial solutions for wide output voltage EV charging are available, such as the ABB Terra 53/54 50 kW, ENERCON E-charger 600 [66], ABB Terra 184 CC HVC, and Porsche charge box [67]. The proposed topology has not been used in the commercially available EV chargers of which the topology is known [66], [67]. On top of that, none of these EV chargers use an isolated topology which would be likely to achieve high efficiencies over the entire output voltage and power range, which makes the proposed two-stage converter unique.

This article proposes a new two-stage reconfigurable LLC resonant converter cascaded with interleaved triangular current mode (TCM) buck converter to address the shortcomings. Fig. 2 shows the two possible configurations of the proposed converter. This converter is capable of a wide output voltage range operation ($150-1000$ V) that enables the charging of both the 400 and 800 V EVs. The LLC full-bridge converter stage is operated at the resonant frequency to benefit from the high efficiency and easy design. By having the interleaved TCM buck converter for the second stage, the turn-on switching loss can be eliminated and the efficiency can be improved due to ZVS [18]. The interleaving also reduces the current stresses (and thereby conduction losses) for the individual TCM buck converter [19], and it allows the large output current ripple of a single TCM buck converter to be partially attenuated, reducing the required dc-link output capacitance. Moreover, the reconfigurable structure allows the secondary sides to be connected in parallel or in series, depending on the output voltage conditions [15]. With this structure, the interleaved buck converter can be operated with a high duty cycle even when the output voltage is low, which results in higher efficiency performance.

The contribution of this article is as follows.

1) A two-stage LLC converter cascaded with interleaved TCM buck converter with a reconfigurable structure is proposed in this article, allowing for a wide output voltage range while maintaining high efficiency over the entire load range.
2) The complete design guidelines including the steady-stage analytical model of the converter are presented. The two possible arrangements and the choice of transistor technologies for the proposed converter are comprehensively evaluated.
3) The proposed converter is experimentally verified, and the performance benchmark of the proposed converter and the conventional frequency modulated LLC converter for the wide output voltage range (150–1000 V) EV charging application is presented. This design benchmark is particularly important because it identifies the proposed converter as an outstanding solution for the future EV market without compromising efficiency.

The structure of the rest of the article is as follows. Section II discusses the operating principle of the proposed two-stage converter. Furthermore, in Sections III and IV, the steady-state analytical models of both the LLC converter and the interleaved TCM buck converter are presented,

respectively. The details regarding the design of both converters are presented in Section V. The results of the analytical comparison of the two possible configurations of the two-stage converter based on the analytical models are presented in Section VI. In Section VII a comparison is made between the proposed converter and the conventional LLC operating using PFM, which is called rLLC PFM in this article. And finally, the results of the experimental verification of the selected configuration are presented in Section VIII.

II. Operating Principle of the Two-Stage Converter

One of the enablers of the wide output voltage range two-stage converter proposed in this study is the voltage-doubler/current-doubler (VD/CD) reconfigurable structure. This structure allows to either connect the two TCM buck outputs in series (to achieve between 500 and 1000 V) to charge the 600 or 800 V batteries, or in parallel (to achieve 150–500 V) to charge the 400 V or lower voltage batteries. And this flexibility in connection is beneficial because the efficiency of the buck converter decreases with decreasing duty cycle D, and the range of the duty cycle during the charging process can be reduced by half by using the VD/CD reconfigurable structure. Consequently, this structure allows the maximum efficiency to be achieved twice in the whole output voltage range. This is especially advantageous since both the 400 V as well as the 800 V battery architectures can be charged with similarly high efficiency.

The operating principle of the reconfigurable structure is as follows: during the communication period in an EV charging session, the EV will inform the charger about the required charging voltage and current value [62]. By comparing the voltage value to a preset boundary voltage value V_{re}, the proposed two-stage LLC converter can be configured into a parallel connection configuration if the required charging voltage value is lower than 500 V or as a series connection if the value is higher than 500 V, by setting the states of the auxiliary switches $S_{\text{aux},1,2,3}$. This connection configuration is done before the start of the charging session, and thus the commutation occurs at zero current.

If there are EVs with a voltage range across 500 V, the sudden change of capacitor voltage due to the dynamic reconfiguration can be avoided by implementing a simple shutdown–reconfiguration-restart mechanism in the controller of the charger. During the energy transferring process, the communication between the vehicle and the charger is still on, and the vehicle continues to send a setting value of charging current or voltage to the dc EV charging station throughout the charging process [62]. Once the charging voltage reaches 500 V, which is the reconfiguration value of the converter, the charger executes a shutdown process. Once the shutdown process is finished, the charging current is zero, and the contactors of the dc power lines are open, the converter can be configurated from the parallel connection into the series connection. Then the energy transferring process is resumed. Another approach is that the conventional frequency modulation can be implemented in the LLC converter stage. By adjusting the switching frequency the converter can cover the exceeding battery voltage range.

The two settings of the auxiliary switches are described below.

A. Series Connection

When $S_{\text{aux},1}$ is kept on while $S_{\text{aux},2,3}$ are maintained off, the negative rail of the upper converter transformer's secondary-side rectifier is connected with the positive rail of the lower side converter rectifier, making the two secondary side circuits connected in series. This configuration enables the converter to supply high output voltage with the utilization of diodes and capacitors with halved voltage rating compared to those of the conventional approach.

B. Parallel Connection

When $S_{\text{aux},1}$ is kept off while $S_{\text{aux},2,3}$ are maintained on, both the transformer's secondary side rectifiers of the converters are connected in parallel. This configuration enables the converter to operate in the low output voltage range <500 V.

Two locations exist where the VD/CD structure can be implemented: After the interleaved TCM buck converter (configuration I), or after the LLC converter (configuration II). See Fig. 2(a) and (b), respectively, for a schematic of both configurations.

The VD/CD structure can be either implemented with solid-state switches or mechanical relays. A benchmarking between both circuits shown in Fig. 2(a) and (b) will be presented in Section VI. First, the analytical models of the LLC converter and TCM buck converter are presented in Sections III and IV, respectively.

III. Steady-State Analytical Modeling of the LLC Converter

The LLC converter operates at a fixed switching frequency slightly above the series resonant frequency $f_{\text{sr}} = 1/(L_r C_r)^{1/2}$. A simplified analysis technique to represent the LLC converter operating close to f_{sr} is the fundamental harmonic approximation (FHA) [20]. This approximation enables classic ac analysis to be used by reducing the entire secondary side of the LLC converter to an equivalent ac resistance R_{ac}.

All equations regarding the LLC converter are listed in Table II. R_L is the load resistance after the rectifier, which is given by (22) for this two-stage converter. The input impedance Z_{in} can be seen as the impedance seen from the primary side full bridge toward the secondary side. For an explanation of M_v, Z_o and Q_L the reader is referred to [20]. The rest of the parameters given in Table II can be found in Fig. 2.

Fig. 3 shows the typical operational waveforms of the LLC converter in resonant frequency.

A. Soft Switching

The LLC converter can achieve ZVS turn-on of the primary side switches. Due to the operation of the converter just above f_{sr}, where the input impedance of the resonant tank network (RTN) is inductive, ZVS is achieved in all primary side switches for the entire load range of the LLC converter.

The maximum magnetizing inductance L_m that allows the output capacitances to be completely charged/discharged

TABLE II
ALL EQUATIONS ON WHICH THE ANALYTICAL MODEL OF THE LLC CONVERTER IS BASED

Description	Parameter	Equation	
Equivalent AC Resistance	R_{AC}	$\frac{8n^2R_L}{\pi^2}$	(1)
Equivalent load resistance	R_{L}	$\frac{(2\cdot V_{\mathrm{link}})^2}{P_{\mathrm{o}}}$	(2)
Voltage gain	M_{v}	$\frac{1}{\sqrt{\left(1+l-l\cdot\left(\frac{\omega_0}{\omega}\right)^2\right)^2+Q_L^2\cdot\left(\frac{\omega}{\omega_0}-\frac{\omega_0}{\omega}\right)^2}}$	(3)
Inductance Ratio	l	$\frac{L_{\mathrm{r}}}{L_{\mathrm{m}}}$	(4)
Characteristic Impedance	Z_{o}	$\sqrt{\frac{L_r}{C_r}}$	(5)
Quality Factor	Q_{L}	$\frac{Z_0}{R_{\mathrm{AC}}}$	(6)
Amplitude of Input Impedance	$\lvert Z_{\mathrm{in}}\rvert$	$\sqrt{\frac{64L_m^2R_L^2n^4}{64R_L^2n^4L_rC_r+L_m\pi^2}}$	(7)
Angle of Input Impedance	$\angle Z_{\mathrm{in}}$	$\arctan\left(\frac{8\sqrt{L_rC_r}n^2}{L_m\pi^2}\frac{V_o^2}{P_o}\right)$	(8)
Series Inductor RMS current	$I_{\mathrm{Lr,RMS}}$	$\frac{4}{\pi}\frac{1}{\sqrt{2}}\frac{V_{\mathrm{in}}}{\lvert Z_{\mathrm{in}}\rvert}$	(9)
Magnetizing RMS current	$I_{\mathrm{Lm,RMS}}$	$\frac{4V_{\mathrm{in}}}{\pi\sqrt{2}}\frac{M_{\mathrm{v}}}{\omega L_m}$	(10)
Maximum resonant Capacitor voltage	$V_{\mathrm{Cr,max}}$	$\frac{1}{\omega C_r}\sqrt{2}I_{\mathrm{Lr,RMS}}$	(11)
Switch turn-on current	$I_{\mathrm{Sx,on}}$	$-\sqrt{2}I_{\mathrm{Lr,RMS}}\sin\left(\angle Z_{\mathrm{in}}\right)$	(12)
Switch turn-off current	$I_{\mathrm{Sx,off}}$	$\sqrt{2}I_{\mathrm{Lr,RMS}}\sin\left(\angle Z_{\mathrm{in}}\right)$	(13)
RMS switch current	$I_{\mathrm{Sx,RMS}}$	$\frac{\sqrt{2}I_{\mathrm{Lr,RMS}}}{2\sqrt{\pi}}\sqrt{\cos\left(\angle Z_{\mathrm{in}}\right)\sin\left(\angle Z_{\mathrm{in}}\right)+\left(\pi-\angle Z_{\mathrm{in}}\right)}$	(14)
Average switch current	$I_{\mathrm{Sx,avg}}$	$\sqrt{2}I_{\mathrm{Lr,RMS}}\frac{\cos\left(\angle Z_{\mathrm{in}}\right)+1}{2\pi}$	(15)
RMS switch bodydiode current	$I_{\mathrm{bd,RMS}}$	$\frac{\sqrt{2}I_{\mathrm{Lr,RMS}}}{2\sqrt{\pi}}\sqrt{-\cos\left(\angle Z_{\mathrm{in}}\right)\sin\left(\angle Z_{\mathrm{in}}\right)+\angle Z_{\mathrm{in}}}$	(16)
Average switch bodydiode current	$I_{\mathrm{bd,avg}}$	$\sqrt{2}I_{\mathrm{Lr,RMS}}\frac{\cos\left(\angle Z_{\mathrm{in}}\right)-1}{2\pi}$	(17)
Average 'rectifier Diode' current	$I_{\mathrm{D,avg}}$	$\frac{1}{2}\frac{P_{\mathrm{o}}}{V_{\mathrm{link}}}$	(18)
RMS 'rectifier Diode' current	$I_{\mathrm{D,RMS}}$	$\frac{\pi}{2}I_{\mathrm{D,avg}}$	(19)
RMS DC-link capacitor current	$I_{\mathrm{Clink,RMS}}$	$\frac{1}{2}\frac{P_{\mathrm{o}}}{V_{\mathrm{o}}}\sqrt{\frac{\pi^2}{8}-1}$	(20)

within a given deadtime is given by the following equation [21]:

$$L_{m,\max}=\frac{t_{\mathrm{dead}}}{16\cdot C_{\mathrm{equi}}f_{\mathrm{sw}}} \tag{21}$$

where C_{equi} is the equivalent representation of all output capacitances C_{oss}. Which is calculated based on the method proposed by Kasper et al. [22].

$$C_{\mathrm{equi}}=4\cdot C_{\mathrm{oss}}. \tag{22}$$

IV. STEADY STATE ANALYTICAL MODELING OF THE INTERLEAVED TCM BUCK CONVERTER

The TCM buck is a synchronous buck converter, as shown in Fig. 4. All equations of the analytical model of the TCM buck converter used in this article are given in Table III.

Fig. 5 shows the typical operational waveforms of a TCM buck converter. In the top graph of Fig. 5 it can be observed that the current through the inductor I_{Lb} can reverse its direction (become negative). The current continues to turn negative until $I_{\mathrm{Lb}}=-I_R$ is reached. At this point, S2 turns off, and the converter enters a period in which a resonant transition occurs (see Section IV-A). After this, I_{Lb} will flow through the body diode of S1 (see Fig. 4), allowing for ZVS turn-on at t_1. The TCM buck converter also achieves ZVS turn-on of S2, in the same way as the regular buck converter.

A. Deadtime Analysis

The process of charging and discharging the output capacitances C_{oss} occurs by means of resonance in the synchronous buck converter. The equivalent circuit during deadtime is shown in Fig. 6.

ZVS turn-on of S1 does not occur in a certain range of I_R, and whether it is achieved can be determined by numerically solving the equations for a series resonant circuit, given in Appendix. By solving these equations it can be seen in Fig. 7 that C_{eq} is not always fully charged/discharged for every combination of t_{dead} and I_R.

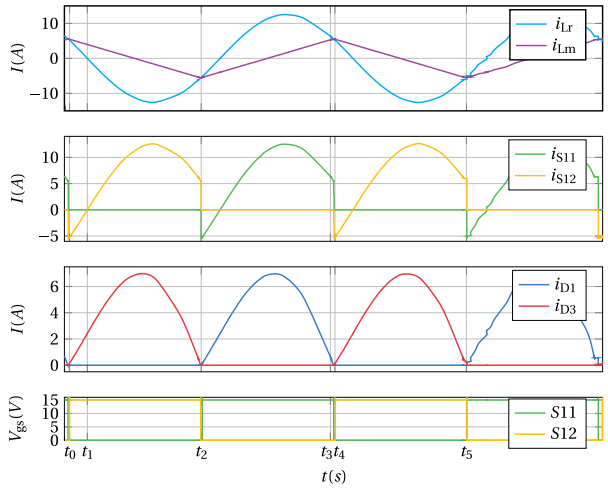

Fig. 3. Operational waveforms of the LLC converter, which is the first stage in the proposed two-stage converter. The series resonant current i_{Lr} and magnetizing current i_{Lm} are given in the top graph, i_{S1} and i_{S2} are the drain-to-source currents of S11 and S12, respectively, and currents through diode D1 and D3 are given in the third graph. The final graph shows the gate-to-source voltage V_{gs} of S11 and S12. See Fig. 2(a) and (b) for reference.

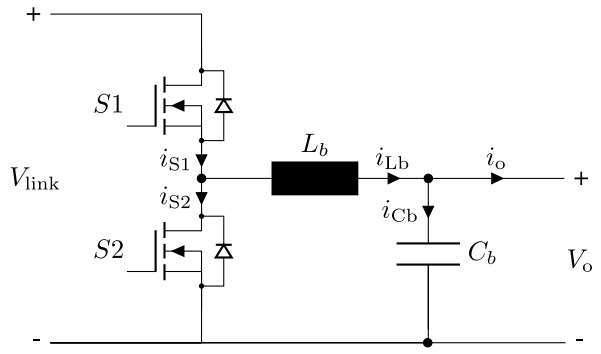

Fig. 4. Schematic of a single TCM buck converter.

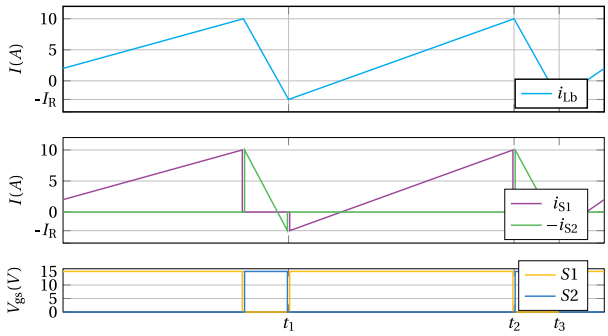

Fig. 5. Operational waveforms of a TCM buck converter, the building block of the second stage in the proposed two-stage converter. i_{Lb} is the current through the inductor of the buck converter, i_{S1} and i_{S2} are the currents through the top and bottom switch of the half-bridge, respectively. See Fig. 4.

V. Converter Design

A. Design Requirements

The design requirements are listed in Table IV, where the targets for $\Delta I_{o,\max}$, $\Delta V_{o,\max}$ and T_{ambient} are taken from dc charging station standard IEC-61851-23:2014 [23].

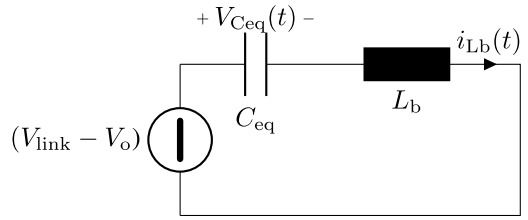

Fig. 6. Equivalent circuit of the TCM buck converter during deadtime. This is a series resonant circuit.

B. Semiconductor Selection

1) LLC Converter: Applying the analytical equations from Table II, the maximum average current stress of the switch for the LLC converter can be approximated to be $\hat{I}_{\text{sw,avg}} = 8.59$ A. And assuming that each switch conducts exactly half of the positive sine wave, the maximum rms current stress on the switches can be calculated to be $\hat{I}_{\text{sw,rms}} = 13.5$ A.

A range of different 1200 V commercial MOSFET and insulated gate bipolar transistor (IGBT) devices that suit these requirements are compared. The switches that would result in the lowest losses for the LLC converter are selected.

1) *LLC IGBT Version:* IKW40N120CS6 from Infineon.
2) *LLC MOSFET Version:* IMW120R060M1 from Infineon.

2) Interleaved TCM Buck Converter: The maximum output current is $I_{o,\max} = 30$ A. Since $N_{\text{phase}} \geq 2$, the average output current of a single buck converter is, therefore, maximum 15 A. Taking the conservative values of $I_R = -5$ A and $D = 1$, the maximum current stress of the interleaved TCM buck converter switch can be calculated using (26), (29) and (31) to be $I_{\text{S1,rms}} = 18.93$ A.

The requirements for the switches in the interleaved TCM buck converter in configuration one are equal to the requirements for the switches of the LLC converter. Therefore the same two switches are selected: as IGBT the IKW40N120CS6 and as MOSFET the IMW120R060M1.

C. Resonant Capacitors

The resonant capacitors in the LLC converter are subject to the total transformer current. The maximum voltage amplitude across the capacitor is calculated using (11). The maximum $I_{\text{Lr,rms}}$ follows from the design script and is equal to 20 Arms. The capacitor bank is arranged with N_p parallel capacitors to lower the rms current on an individual capacitor. The selected resonant capacitor is the B32671L6473K000: (47 nF). These capacitors have a dc voltage rating of 630 V, with no derating required at $f_{\text{sw}} = 15$ kHz. The required voltage rating, using (11), is only ≈200 V (peak). The number of parallel capacitors to achieve the required C_r is 33.

D. Transformer Design

The operating frequency of the LLC converter is relatively low ($f_{\text{sw,LLC}} = 15$ kHz), as stated in Table IV. This low frequency and high power naturally results in the requirement of large area-product cores. The minimal number of turns of

TABLE III
ALL EQUATIONS ON WHICH THE ANALYTICAL MODEL OF THE TCM BUCK CONVERTER IS BASED

Description	Definition	
Dutycycle	$\mathrm{D} = \mathrm{V_o}/V_{\mathrm{in}}$	(23)
Switching frequency	$\mathrm{f_{sw}} = \frac{1}{L_\mathrm{b}} \cdot D \cdot \frac{V_{\mathrm{in}} - V_{\mathrm{out}}}{2(I_\mathrm{o} + I_\mathrm{R})}$	(24)
Average Inductor Current	$\mathrm{I_{Lb,avg}} = I_\mathrm{o}$	(25)
Peak-to-Peak Inductor Current	$\mathrm{I_{Lb,pk-pk}} = 2(I_\mathrm{o} + \lvert I_\mathrm{R}\rvert)$	(26)
Maximum Inductor Current	$\mathrm{I_{Lb,max}} = 2(I_\mathrm{o} + \frac{1}{2}\lvert I_\mathrm{R}\rvert)$	(27)
RMS Inductor Current	$\mathrm{I_{Lb,rms}} = \sqrt{\frac{1}{3} I^2_{\mathrm{Lb,pk-pk}} - I_\mathrm{R} I_{\mathrm{Lb,pk-pk}} + I^2_\mathrm{R}}$	(28)
	$\mathrm{k_1} = \lvert I_\mathrm{R}\rvert / I_{\mathrm{Lb,pk-pk}}$	(29)
Average high-side switch current	$\mathrm{I_{S1,avg}} = D I_\mathrm{o}$	(30)
RMS high-side switch current	$\mathrm{I_{S1,RMS}} = \sqrt{\left(I_\mathrm{R}\sqrt{D\frac{k_1}{3}}\right)^2 + \left(I_{\mathrm{Lb,max}}\sqrt{D\frac{1-k_1}{3}}\right)^2}$	(31)
Average low-side switch current	$\mathrm{I_{S2,avg}} = (1-D) I_\mathrm{o}$	(32)
RMS low-side switch current	$\mathrm{I_{S2,RMS}} = \sqrt{\left(I_\mathrm{R}\sqrt{(1-D)\frac{k_1}{3}}\right)^2 + \left(I_{\mathrm{Lb,max}}\sqrt{(1-D)\frac{1-k_1}{3}}\right)^2}$	(33)
Turn-off current high-side switch	$\mathrm{I_{S1,off}} = I_{\mathrm{Lb,max}}$	(34)
Turn-off current low-side switch	$\mathrm{I_{S2,off}} = I_\mathrm{R}$	(35)
Interleaved output current ripple	$\Delta I_\mathrm{o} = \frac{V_{\mathrm{in}} D}{f_{\mathrm{sw}}} \left(1 - \frac{\lfloor N_{\mathrm{phase}} D \rfloor}{N_{\mathrm{phase}} D}\right) \left(1 + \lfloor N_{\mathrm{phase}} D \rfloor - N_{\mathrm{phase}} D\right)$	(36)
Output capacitor RMS current	$\mathrm{I_{Cb,rms}} = \sqrt{\frac{\Delta I_\mathrm{o}^2}{12}}$	(37)

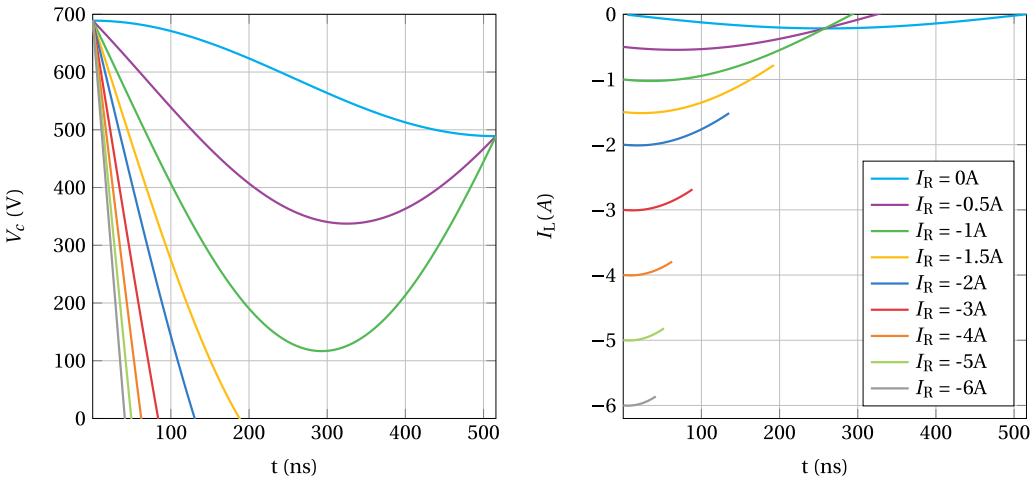

Fig. 7. Voltage across the equivalent capacitance C_{eq} of Fig. 6 and the current through the inductor L_b at that same time in the resonant interval during t_{dead}. ZVS is only achieved when $V_c = 0\,\mathrm{V}$. This figure shows that not all values of I_R will lead to ZVS. $V_{\mathrm{in}} = 689\,\mathrm{V}$, $V_o = 100\,\mathrm{V}$, $C = 355\,\mathrm{pF}$, $L = 75.8\ \mu\mathrm{H}$.

the primary side winding can be calculated by the following equation:

$$N_{\mathrm{min}} = \frac{V_{\mathrm{in}}}{4 \cdot A_c \cdot B_{\mathrm{op}} \cdot f_{\mathrm{sw}}}. \tag{38}$$

An airgap might be required to lower the magnetizing inductance value L_m, required to satisfy ZVS requirements of the LLC converter. The relationship between the airgap length and the magnetizing inductance can be approximated by the following equation:

$$L \approx \frac{N^2}{R_g} \approx \frac{N^2}{2 \cdot l_{\mathrm{air}}/\mu_0 A_c}. \tag{39}$$

The winding losses are calculated in MATLAB based on the procedure described by Mühlethaler [24], and the core losses are calculated using the improved generalized steinmetz equation (iGSE) [24], [65]. The details are not further elaborated upon in this work.

TABLE IV
DESIGN REQUIREMENTS FOR THE WIDE OUTPUT VOLTAGE RANGE RESONANT CONVERTER

Parameter	Symbol	Value
Input voltage range	V_{in}	640-840 V
Output voltage range	V_{out}	150-1000 V
Switching frequency LLC	$f_{\text{sw,LLC}}$	15 kHz
Maximum output power	$P_{\text{o,max}}$	11 kW
Maximum output current	$I_{\text{o,max}}$	30 A
Maximum output current ripple during CC*	$\Delta I_{\text{o,max}}$	9 A
Maximum output voltage ripple during CV*	$\Delta V_{\text{o,max}}$	10 V
Operating temperature range	T_{ambient}	−5-40 °C

E. Inductor Design

The work in [15] is used for designing the four inductors of the interleaved TCM buck converter and the external resonant inductor $L_{r,\text{ext}}$ of the LLC converter. The minimum number of turns can be calculated using (40), and the required airgap length l_g to achieve the required inductance can be calculated by (41)

$$N_{\text{min}} = \frac{\text{LI}_{\text{max}}}{B_{\text{max}} A_c} \tag{40}$$

$$l_g = \frac{\text{LI}^2_{\text{max}} \mu_0}{B^2_{\text{max}} A_c}. \tag{41}$$

The winding losses and core loss are, again, calculated in MATLAB based on the procedure described in [24], and [65].

F. Design Summary

The selection choices of all other components of the proposed converter are summarized in Tables V and VI. The output capacitors of the interleaved TCM buck converter are selected to meet the requirements from IEC-61851-23:2014 [23] (see Table IV).

VI. RESULTS OF THE ANALYTICAL COMPARISON

In order to compare the efficiency performance of the two possible configurations presented in Fig. 2, the charging-cycle efficiency [15] is used, which represents the average efficiency of the converter over the whole charging process.

As explained in Section II, two possible configurations of the two-stage converter were compared together with the use of either SiC MOSFETs or IGBTs. The results for the first stage, the LLC converter, are given in Section VI-A, while the results of the interleaved TCM buck converter configuration comparison are given in Section VI-B.

A. LLC Converter

For the LLC converter in this article only a comparison was made between a SiC MOSFET based or IGBT based LLC converter. The performance of the converter was measured based on the charging cycle efficiencies, as explained in [15]. Table VII indicates that the efficiency of both the SiC MOSFET based and IGBT based LLC converter have approximately the same charging cycle efficiencies, given $f_{\text{sw}} = 15$ kHz. Therefore, the IKW40N120CS6 IGBT version of the LLC converter is selected due to its lower cost.

TABLE V
ALL COMPONENTS IN THE FINAL DESIGN OF THE LLC CONVERTER

Component	Description/Part Number
LLC IGBT's	IKW40N120CS6
Resonant capacitors	B32671L6473K000 (47 nF)
Transformer core shape	EE70/33/32
Number of parallel cores n_{cores}	5
Transformer Airgap	0.3 mm
N_{pri}	20
N_{sec}	30 (2 · 15)
Magnetizing Inductance L_{m}	4.8 mH
External Resonant Inductor Core Shape	EE70/33/32
Number of parallel cores n_{cores}	1
Inductor airgap	1.3 mm
N	14
Resonant Inductance L_{r}	64.43 uH
Rectifier Diodes	IDW30G120C5B
LLC output capacitors	C4AQIBW5600A3NJ (2 · 2·60 uF)

TABLE VI
ALL COMPONENTS IN THE FINAL DESIGN OF THE INTERLEAVED TCM BUCK CONVERTER

Component	Description/Part Number
SiC MOFSET's	IMW120R060M1 (2 · 2 · 2)
Parallel phases per module N_{phase}	2
Inductor core shape	EE70/33/32
Number of parallel cores n_{cores}	1
Inductor airgap	1.6 mm
N	12
buck Inductance L_{b}	75.6 uH
LLC output capacitors	C4AQILW5150A36J (2 · 2·15 uF
Power Relays	TE-T9G ($3x$)

TABLE VII
EFFICIENCY AND LOSSES OF THE 11 kW LLC CONVERTER USING EITHER A MOSFET (IMW120R060M1) OR AN IGBT (IKW40N120CS6) AS TRANSISTOR ($V_{\text{in}} = 840$ V)

Switch Type	Charge Cycle Efficiencies ($\eta(-)$)				
	11 kW 400 V	55 kW 400 V	11 kW 800 V	55 kW 800 V	Average
IMW120R060M1	0.9799	0.9787	0.9798	0.9795	**0.9795**
IKW40N120CS6	0.9796	0.9763	0.9795	0.9786	**0.9784**

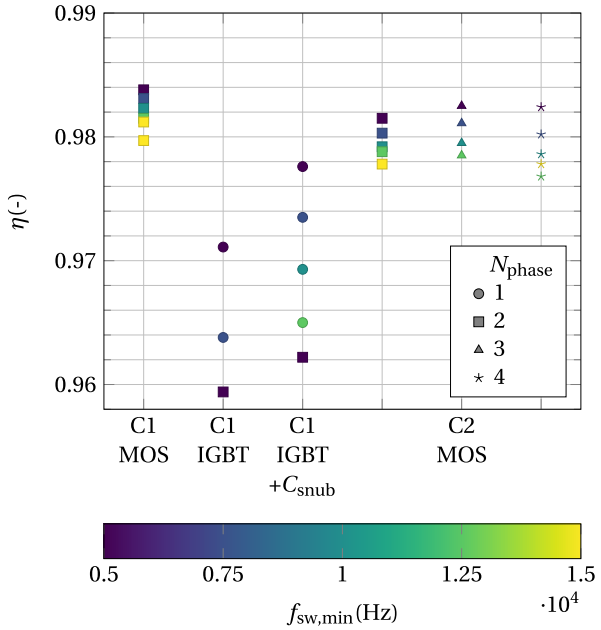

Fig. 8. Average charging cycle efficiency of the interleaved TCM buck converter solution space. $C1$ = configuration 1, and $C2$ = configuration 2.

TABLE VIII
SELECTED FINAL DESIGN OF THE TCM BUCK CONVERTER IN THIS ARTICLE

Design Parameter	Value
Configuration	1
$f_{sw,min}$	15 kHz
Switch technology	MOSFET
Switches	IMW120R060M1
N_{phase}	2

B. Interleaved TCM Buck Converter

The comparison of different design solutions for the interleaved TCM buck converter is more elaborate because a given design solution consists of five different variables.

1) Configuration 1 or 2.
2) Minimum switching frequency [see (24)].
3) IGBT or SiC MOSFET based.
4) Number of interleaved phases per module N_{phase}.

Running the analytical comparison of several possible design solutions and comparing the average efficiency of all four charging cycles proposed in [15] gives us the solution space given in Fig. 8. Note that no competitive IGBT could be found for use in configuration 2 (which requires higher $V_{DS,max}$ than configuration 1) due to the unsatisfactory switching losses performance from the devices available on the market.

It can be seen that the MOSFET-based solutions are more efficient when compared to IGBT-based solutions. And, specifically, configuration 1 using MOSFETs generates the most efficient converters for each respective $f_{sw,min}$. The selected solution for the TCM buck converter in this article is shown in Table VIII.

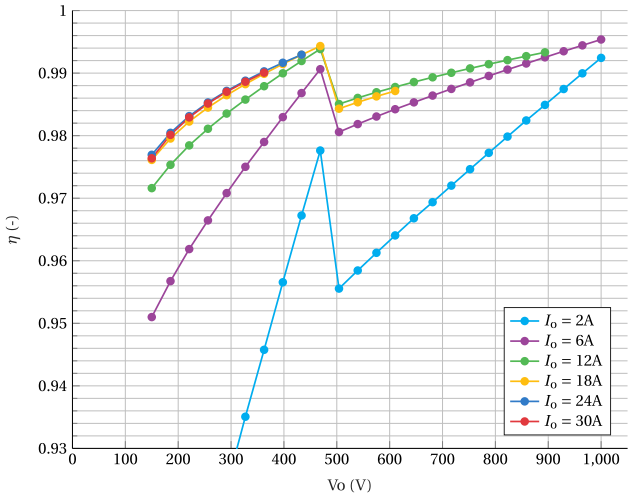

Fig. 9. Analytical efficiency of the TCM buck converter for different I_o over the entire V_o range (with V_{in} = 525 V).

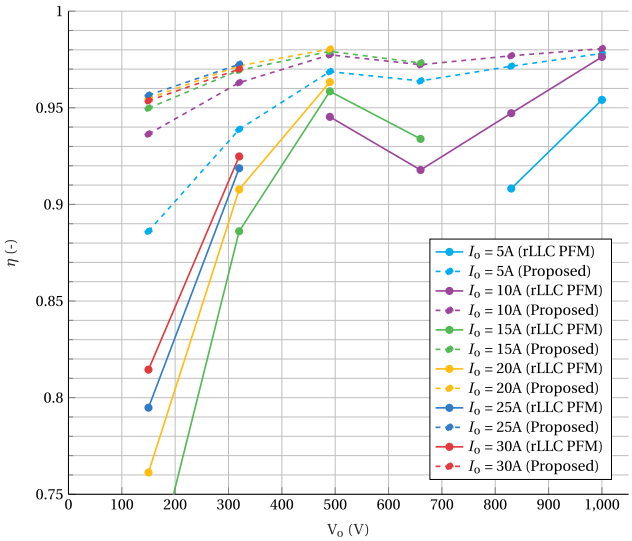

Fig. 10. Analytical efficiency comparison between the proposed solution and the conventional frequency modulated LLC converter (rLLC PFM). The output voltage is on the x-axis, and the colors indicate different I_o.

The reason that IGBT-based converters achieve a lower average efficiency in the TCM buck converter is because of the high switching frequencies operation required for partial loads [see (24)].

The calculated efficiency of the selected design solution of the interleaved TCM buck converter over the entire operating range of the system is shown next to the measured efficiency in Fig. 9.

VII. COMPARISON TO CONVENTIONAL FREQUENCY-MODULATED LLC

In order to emphasize the benefit of the proposed two-stage wide output voltage range EV charger solution, a comparison is made with the conventional frequency-modulated LLC converter. To do this, the buck stage is removed from the two-stage converter shown in Fig. 2(b), however, the re-configurable secondary sides of the LLC are kept to improve efficiency and reduce switching frequency operational range. The proposed

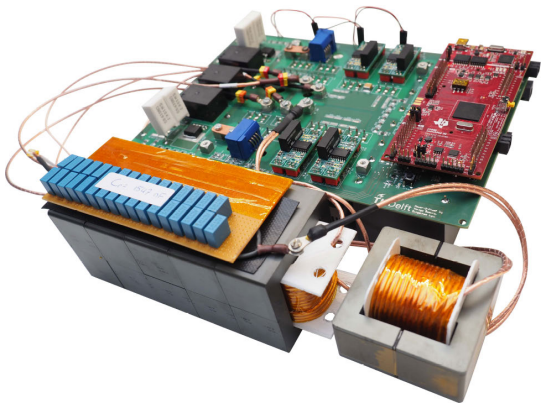

Fig. 11. Designed LLC converter hardware demonstrator.

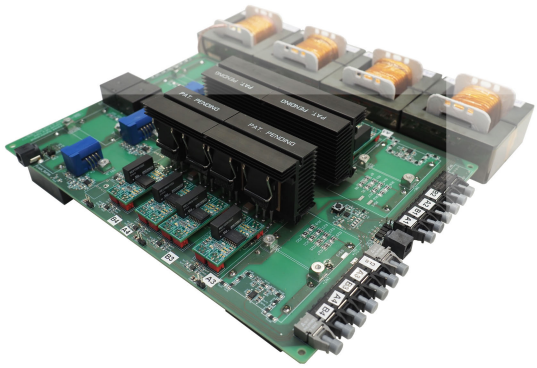

Fig. 12. Designed interleaved TCM buck converter hardware demonstrator.

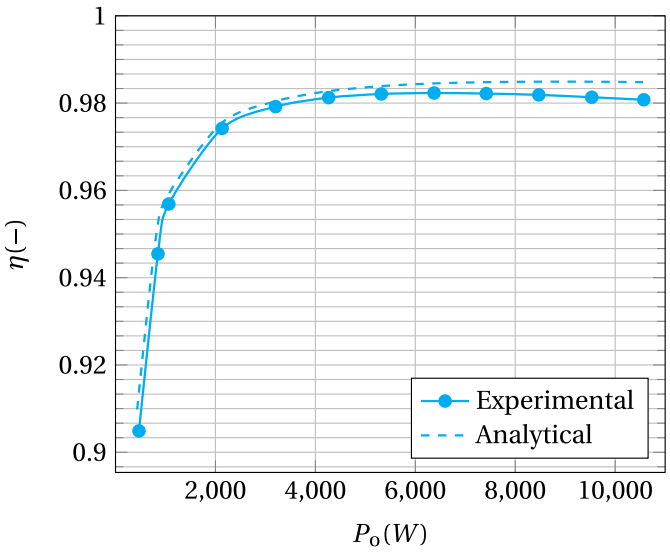

Fig. 13. LLC converter efficiency over the entire output power range P_o as calculated analytically and measured experimentally.

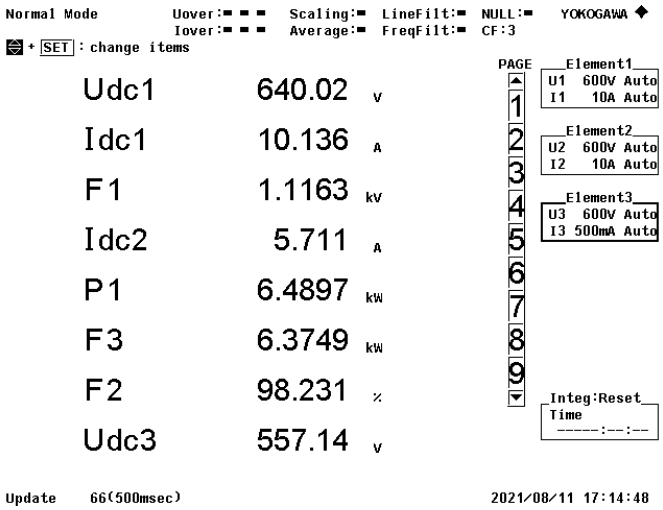

Fig. 14. Screenshot taken on the Yokogawa WT500 power analyzer at the operation point with the highest measured efficiency $P_o = 6.37$ kW.

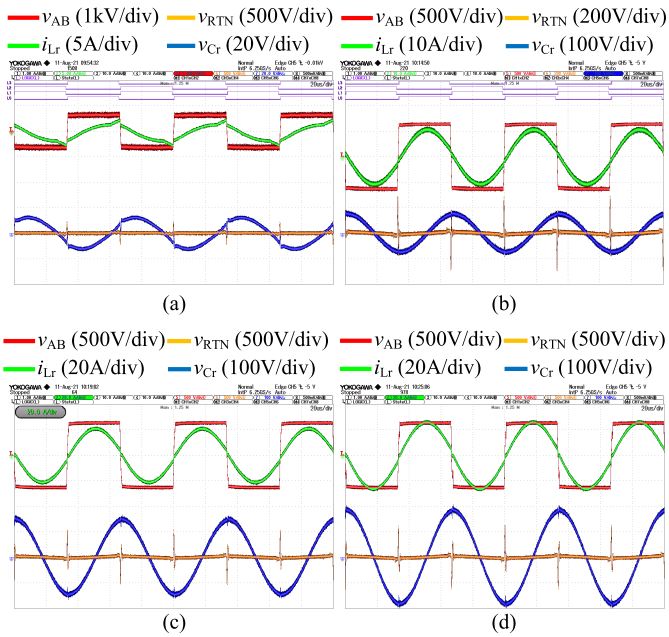

Fig. 15. Operational waveforms of the LLC converter at different output powers P_o, with $V_{in} = 640$ V. i_{Lr} is the current through the resonant inductor, v_{Cr} is the voltage across the resonant capacitor, v_{AB} and v_{RTN} are the terminal voltage from the H-bridge and the voltage across the RTN (the voltage across the series connection of L_r and C_r), respectively. (a) $P = 400$ W. (b) $P = 4$ kW. (c) $P = 8$ kW. (d) $P = 10.5$ kW.

LLC design from Table V is then employed using solely PFM to control the output voltage (rLLC PFM). The analytical efficiency comparison over the entire operational range is shown in Fig. 10.

Judging from Fig. 10, the benefit of the proposed wide output voltage EV charger appears evidently: the proposed solution is highly efficient over the entire operational range, which is not the case for the rLLC PFM. The switching frequency operational range of the rLLC PFM is 4.8–87.3 kHz. Operational points which showed large deviations between the analytical model and LTSpice simulations are not displayed for the rLLC PFM. These were operational points for which the FHA model was not valid. The rLLC PFM deviates from the series resonant frequency operational point, which creates reactive currents in the RTN that cause additional losses. On top of that, the IGBTs need to switch at multiples of the base 15 kHz for some operational points, causing additional switching losses.

This almost flat high-efficiency curve of the proposed solution is enabled due to the unique combination of the

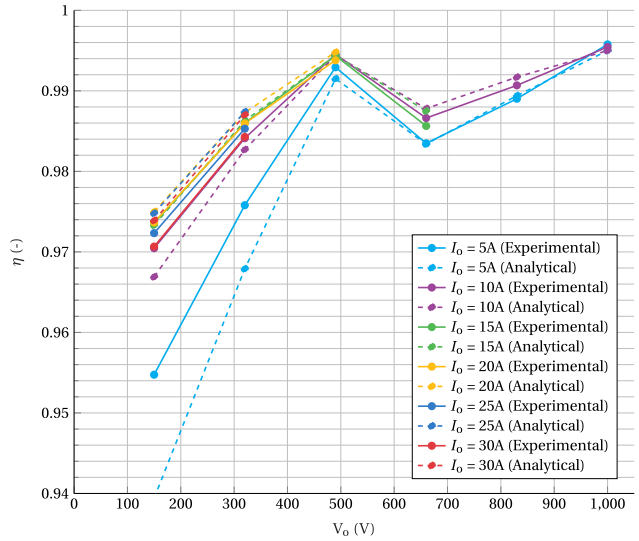

Fig. 16. Comparison of $\eta_{\text{analytical}}$ and η_{measured} for the interleaved TCM Buck converter over the entire operating range. The output voltage is on the x-axis, and the colors indicate different I_o.

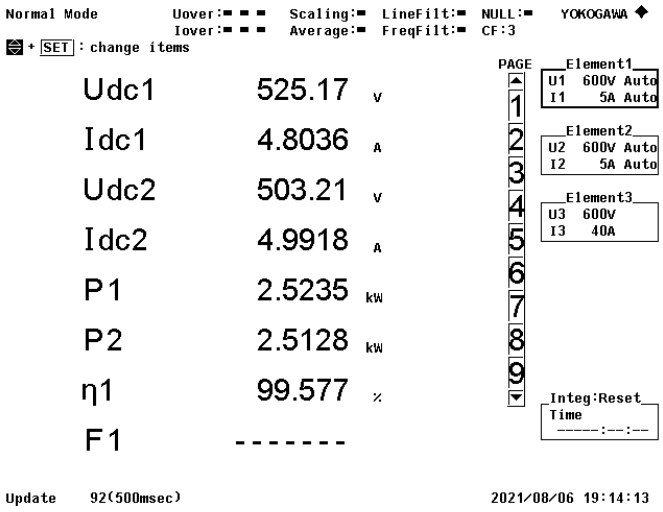

Fig. 17. Screenshot taken on the Yokogawa WT500 Power Analyzer at the operation point with the highest measured efficiency $V_o = 1000\,\text{V}$, $I_o = 5\,\text{A}$.

LLC converter, interleaved TCM Buck converter, and reconfigurable stage, resulting in the highest reported output voltage range for a resonant converter-based EV charger while maintaining this almost flat high-efficiency curve.

VIII. Experimental Results

The selected design solutions for the LLC converter and interleaved TCM buck converter are verified experimentally. Figs. 11 and 12 present the hardware demonstrators of the LLC converter and interleaved TCM buck converter, respectively.

A. LLC Converter

The experimentally measured efficiency of the LLC converter over the load range from 400 W to 11 kW with an input voltage of 640 V is shown in Fig. 13. The peak efficiency of the LLC converter is 98.231% at $P_o = 6.37\,\text{kW}$; see Fig. 14.

The measured operational waveforms at different output powers of the LLC converter are shown in Fig. 15.

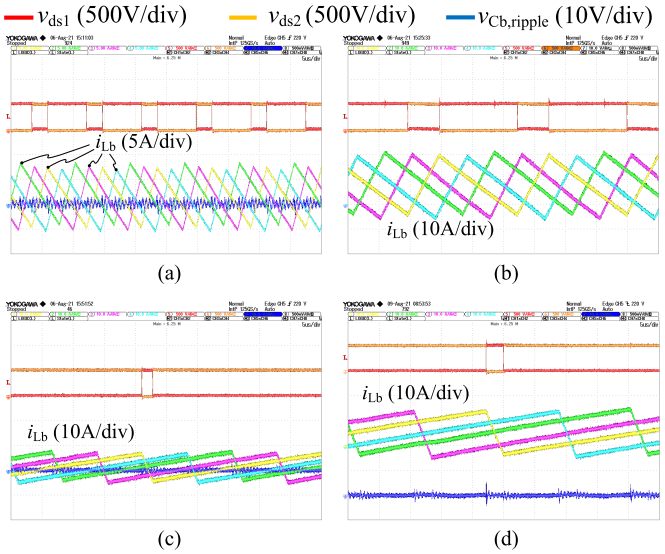

Fig. 18. Operational waveform of the interleaved TCM buck converter in current-doubler mode in different output voltage and current, with $V_{\text{in}} = 525$ V. v_{ds1} is the drain–source voltage on the high-side MOSFET, v_{ds2} is the drain–source voltage on the low-side MOSFET, $v_{\text{Cb,ripple}}$ is the voltage ripple on the output capacitor C_b. (a) $V_{\text{out}} = 150$ V, $I_{\text{out}} = 5$ A, $f_{\text{sw}} = 113.4$ kHz. (b) $V_{\text{out}} = 150$ V, $I_{\text{out}} = 30$ A, $f_{\text{sw}} = 56.7$ kHz. (c) $V_{\text{out}} = 490$ V, $I_{\text{out}} = 5$ A, $f_{\text{sw}} = 34.6$ kHz. (d) $V_{\text{out}} = 490$ V, $I_{\text{out}} = 20$ A, $f_{\text{sw}} = 21.6$ kHz.

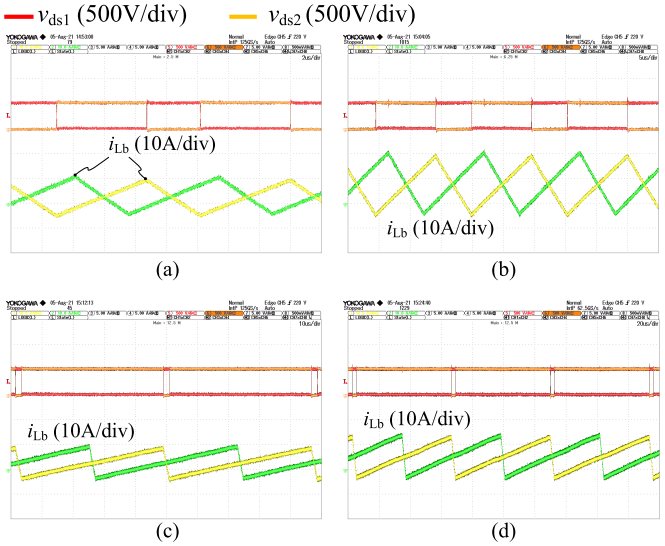

Fig. 19. Operational waveform of the interleaved TCM buck converters in voltage-doubler mode in different output voltage and current, with $V_{\text{in}} = 525$ V. v_{ds1} is the drain–source voltage on the high-side MOSFET, v_{ds2} is the drain–source voltage on the low-side MOSFET. (a) $V_{\text{out}} = 660$ V, $I_{\text{out}} = 5$ A, $f_{\text{sw}} = 108.1$ kHz. (b) $V_{\text{out}} = 660$ V, $I_{\text{out}} = 15$ A, $f_{\text{sw}} = 64.9$ kHz. (c) $V_{\text{out}} = 1$ kV, $I_{\text{out}} = 5$ A, $f_{\text{sw}} = 21$ kHz. (d) $V_{\text{out}} = 1$ kV, $I_{\text{out}} = 10$ A, $f_{\text{sw}} = 15.8$ kHz.

B. Interleaved TCM Buck Converter

The efficiency of the selected interleaved TCM buck converter solution presented in Table VIII is measured. The results are given in Fig. 16, where they are compared with the calculated efficiency. The peak efficiency is measured at $V_o = 1000\,\text{V}$ and $I_o = 5\,\text{A}$ at 99.577%, as can be observed in Fig. 17.

The waveforms of the interleaved TCM buck converter at different operating points are given in Figs. 18 and 19. The converter is placed in current-doubler mode in Fig. 18, and

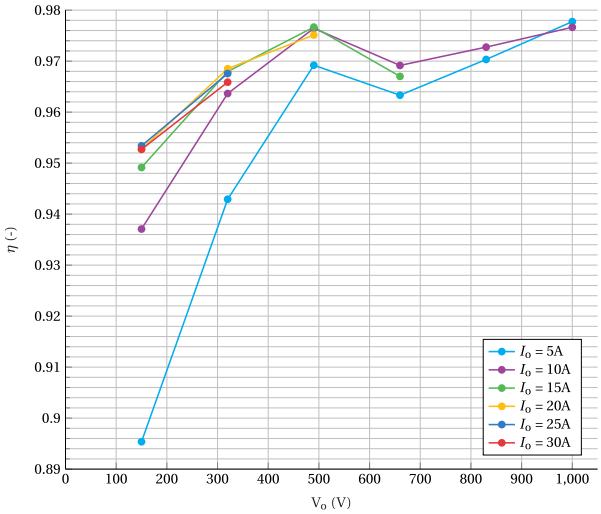

Fig. 20. Measured efficiency of the two-stage LLC + interleaved TCM buck converter over the entire operating range. The efficiencies of the interleaved TCM buck converter in Fig. 16 are multiplied by the (interpolated) efficiency of the LLC converter determined from Fig. 13 to obtain the efficiency of the two-stage converter.

in voltage-doubler mode in Fig. 19 Note that, the data shown for the voltage-doubler mode is measured only in one of the interleaved TCM buck converters.

C. Two-Stage Converter Efficiency

The power efficiencies of the two individual stages were given in the previous sections, Sections VIII-A and VIII-B. Combining the power efficiencies given in these sections gives the total efficiency of the proposed two-stage converter in Fig. 20, achieving a peak efficiency of 97.66%.

IX. Conclusion

The aim of the current study was to propose an 11 kW dc-dc converter that is suited for EV charging with a wide output voltage range with very high efficiency over the entire operational range based on an RPC topology. The implemented solution consisted of a two-stage power converter. This is based on an LLC resonant converter followed by an interleaved TCM buck converter. The achieved output voltage range of 150–1000 V in the current study was not previously reported in the literature regarding RPCs for EV charging. And therefore, the proposed converter is capable of charging different EV battery types while doing so very efficiently. A prototype of the proposed converter was designed and used to evaluate the efficiency: >95% efficiency was achieved over the entire output voltage range at maximum power, with a peak efficiency of 97.66%. The obtained efficiency for the 11 kW-400 V Charging cycle is 96.85% and 95.67% for the 11 kW-800 V charging cycle.

Appendix
Series Resonant Circuit

Applying KVL and KCL to the equivalent circuit results in the differential equations for $V_{C,\mathrm{eq}}(t)$ and $I_{\mathrm{Lb}}(t)$

$$\begin{aligned} V_{C,\mathrm{eq}}(t) &= (V_{\mathrm{in}} - V_o) - ((V_{\mathrm{in}} - V_o) - V_{c0})\cos(t - t_0) \\ &\quad + Z_0 \cdot I_{L0}\sin(\omega_0(t - t_0)) \\ &= (V_{\mathrm{in}} - V_o) + V_o\cos(t - t_0) \\ &\quad + Z_0 \cdot I_{L0}\sin(\omega_0(t - t_0)) \qquad (42) \end{aligned}$$

$$I_{\mathrm{Lb}}(t) = (V_{\mathrm{in}} - V_o) + Z_0 \cdot I_{L0} \cdot \sin(w_0 \cdot t_{\mathrm{dead}}). \qquad (43)$$

References

[1] *Paris Agreement (English)*. United Nations. Accessed: Dec. 20, 2021. [Online]. Available: https://unfccc.int/documents/37107

[2] International Energy Agency (IEA). *Global EV Outlook 2021—Accelerating Ambitions Despite the Pandemic*. Accessed: Jul. 28, 2021. [Online]. Available: https://iea.blob.core.windows.net/assets/ed5f4484-f556-4110-8c5c-4ede8bcba637/GlobalEVOutlook2021.pdf

[3] IDTechX. *Powertrain Efficiency: Sustaining EV Growth in an Era of Shortages*. Accessed: Jun. 4, 2023. [Online]. Available: https://www.idtechex.com/en/research-article/powertrain-efficiency-sustaining-ev-growth-in-an-era-of-shortages/27367

[4] M. Ahmadi, N. Mithulananthan, and R. Sharma, "A review on topologies for fast charging stations for electric vehicles," in *Proc. IEEE Int. Conf. Power Syst. Technol. (POWERCON)*, Wollongong, NSW, Australia, Sep. 2016, pp. 1–6, doi: 10.1109/POWERCON.2016.7753886.

[5] H. Wang, S. Dusmez, and A. Khaligh, "A novel approach to design EV battery chargers using SEPIC PFC stage and optimal operating point tracking technique for LLC converter," in *Proc. IEEE Appl. Power Electron. Conf. Exposit. (APEC)*, Fort Worth, TX, USA, Mar. 2014, pp. 1683–1689, doi: 10.1109/APEC.2014.6803532.

[6] C. Shi, H. Wang, S. Dusmez, and A. Khaligh, "A SiC-based high-efficiency isolated onboard PEV charger with ultrawide DC-link voltage range," *IEEE Trans. Ind. Appl.*, vol. 53, no. 1, pp. 501–511, Jan. 2017, doi: 10.1109/TIA.2016.2605063.

[7] C. Wei, D. Zhu, H. Xie, Y. Liu, and J. Shao, "A SiC-based 22kW bi-directional CLLC resonant converter with flexible voltage gain control scheme for EV on-board charger," in *Proc. PCIM Eur. Digit. Days Int. Exhib. Conf. Power Electron., Intell. Motion, Renew. Energy Energy Manage.*, Jul. 2020, pp. 1–7.

[8] Y. Xuan, X. Yang, W. Chen, T. Liu, and X. Hao, "A novel three-level CLLC resonant DC–DC converter for bidirectional EV charger in DC microgrids," *IEEE Trans. Ind. Electron.*, vol. 68, no. 3, pp. 2334–2344, Mar. 2021, doi: 10.1109/TIE.2020.2972446.

[9] B. Xue, H. Wang, J. Liang, Q. Cao, and Z. Li, "Phase-shift modulated interleaved LLC converter with ultrawide output voltage range," *IEEE Trans. Power Electron.*, vol. 36, no. 1, pp. 493–503, Jan. 2021, doi: 10.1109/TPEL.2020.3001126.

[10] M. I. Shahzad, S. Iqbal, and S. Taib, "Interleaved LLC converter with cascaded voltage-doubler rectifiers for deeply depleted PEV battery charging," *IEEE Trans. Transport. Electrific.*, vol. 4, no. 1, pp. 89–98, Mar. 2018, doi: 10.1109/TTE.2017.2753407.

[11] W. Lee, J. Kim, J. Lee, and I. Lee, "Design of an isolated DC/DC topology with high efficiency of over 97% for EV fast chargers," *IEEE Trans. Veh. Technol.*, vol. 68, no. 12, pp. 11725–11737, Dec. 2019, doi: 10.1109/TVT.2019.2949080.

[12] Y. Wei, Q. Luo, and A. Mantooth, "Overview of modulation strategies for LLC resonant converter," *IEEE Trans. Power Electron.*, vol. 35, no. 10, pp. 10423–10443, Oct. 2020, doi: 10.1109/TPEL.2020.2975392.

[13] M. Kwon, S. Jung, and S. Choi, "A high efficiency bi-directional EV charger with seamless mode transfer for V2G and V2H application," in *Proc. IEEE Energy Convers. Congr. Exposit. (ECCE)*, Montreal, QC, Canada, Sep. 2015, pp. 5394–5399, doi: 10.1109/ECCE.2015.7310418.

[14] Z. U. Zahid, Z. M. Dalala, R. Chen, B. Chen, and J. Lai, "Design of bidirectional DC–DC resonant converter for vehicle-to-grid (V2G) applications," *IEEE Trans. Transport. Electrific.*, vol. 1, no. 3, pp. 232–244, Oct. 2015, doi: 10.1109/TTE.2015.2476035.

[15] D. Lyu, T. B. Soeiro, and P. Bauer, "Design and implementation of a reconfigurable phase shift full-bridge converter for wide voltage range EV charging application," *IEEE Trans. Transport. Electrific.*, vol. 9, no. 1, pp. 1200–1214, Mar. 2023, doi: 10.1109/TTE.2022.3176826.

[16] Y. Liu, Y. Syu, N. A. Dung, C. Chen, K. Chen, and K. A. Kim, "High-switching-frequency TCM digital control for bidirectional-interleaved buck converters without phase error for battery charging," *IEEE J. Emerg. Sel. Topics Power Electron.*, vol. 8, no. 3, pp. 2111–2123, Sep. 2020, doi: 10.1109/JESTPE.2019.2954602.

[17] C. Yeh, X. Zhao, and J. Lai, "An investigation on zero-voltage-switching condition in synchronous-conduction-mode buck converter," in *Proc. IEEE Energy Convers. Congr. Exposit. (ECCE)*, Oct. 2017, pp. 1728–1732, doi: 10.1109/ECCE.2017.8096002.

[18] D. Christen, S. Tschannen, and J. Biela, "Highly efficient and compact DC–DC converter for ultra-fast charging of electric vehicles," in *Proc. 15th Int. Power Electron. Motion Control Conf. (EPE/PEMC)*, Sep. 2012, pp. 1–8, doi: 10.1109/EPEPEMC.2012.6397481.

[19] Texas Instruments. *Benefits of a Multiphase Buck Converter*. Accessed: Jun. 4, 2023. [Online]. Available: https://www.ti.com/lit/an/slyt449/slyt449.pdf

[20] R. L. Steigerwald, "A comparison of half-bridge resonant converter topologies," *IEEE Trans. Power Electron.*, vol. PE-3, no. 2, pp. 174–182, Apr. 1988, doi: 10.1109/63.4347.

[21] U. Kundu, K. Yenduri, and P. Sensarma, "Accurate ZVS analysis for magnetic design and efficiency improvement of full-bridge LLC resonant converter," *IEEE Trans. Power Electron.*, vol. 32, no. 3, pp. 1703–1706, Mar. 2017, doi: 10.1109/TPEL.2016.2604118.

[22] M. Kasper, R. M. Burkart, G. Deboy, and J. W. Kolar, "ZVS of power MOSFETs revisited," *IEEE Trans. Power Electron.*, vol. 31, no. 12, pp. 8063–8067, Dec. 2016, doi: 10.1109/TPEL.2016.2574998.

[23] *Electric Vehicle Conductive Charging System—Part 23: DC Electric Vehicle Charging Station*, document IEC61851-23:2014, International Electrotechnical Commission, Geneva, Switzerland, 2014.

[24] J. Mühlethaler, "Modeling and multi-objective optimization of inductive power components," Doctoral dissertation, Dep. Inf. Technologie und Elektrotechnik, ETH Zurich, Zurich, Switzerland, 2012, doi: 10.3929/ethz-a-007328104.

[25] C. Jung, "Power up with 800-V systems: The benefits of upgrading voltage power for battery-electric passenger vehicles," *IEEE Electrific. Mag.*, vol. 5, no. 1, pp. 53–58, Mar. 2017, doi: 10.1109/MELE.2016.2644560.

[26] T. B. Soeiro, J. Mühlethaler, J. Linnér, P. Ranstad, and J. W. Kolar, "Automated design of a high-power high-frequency LCC resonant converter for electrostatic precipitators," *IEEE Trans. Ind. Electron.*, vol. 60, no. 11, pp. 4805–4819, Nov. 2013, doi: 10.1109/TIE.2012.2227897.

[27] R. Gadelrab, Y. Yang, B. Li, F. Lee, and Q. Li, "High-frequency high-density bidirectional EV charger," in *Proc. IEEE Transp. Electrific. Conf. Expo. (ITEC)*, Jun. 2018, pp. 687–694, doi: 10.1109/ITEC.2018.8450117.

[28] B. Li, Q. Li, and F. C. Lee, "A WBG based three phase 12.5 kW 500 kHz CLLC resonant converter with integrated PCB winding transformer," in *Proc. IEEE Appl. Power Electron. Conf. Exposit. (APEC)*, Mar. 2018, pp. 469–475, doi: 10.1109/APEC.2018.8341053.

[29] L. A. D. Ta, N. D. Dao, and D. Lee, "High-efficiency hybrid LLC resonant converter for on-board chargers of plug-in electric vehicles," *IEEE Trans. Power Electron.*, vol. 35, no. 8, pp. 8324–8334, Aug. 2020, doi: 10.1109/TPEL.2020.2968084.

[30] C. Shen, Q. Xiao, and Y. Zhang, "High-efficiency design method of LLC resonant converter for PHEV battery chargers (based on time-domain model)," *IET Electr. Syst. Transp.*, vol. 10, no. 3, pp. 234–242, Sep. 2020, doi: 10.1049/iet-est.2019.0092.

[31] H. Wang and Z. Li, "A PWM LLC type resonant converter adapted to wide output range in PEV charging applications," *IEEE Trans. Power Electron.*, vol. 33, no. 5, pp. 3791–3801, May 2018, doi: 10.1109/TPEL.2017.2713815.

[32] Y. Shen, W. Zhao, Z. Chen, and C. Cai, "Full-bridge LLC resonant converter with series-parallel connected transformers for electric vehicle on-board charger," *IEEE Access*, vol. 6, pp. 13490–13500, 2018, doi: 10.1109/ACCESS.2018.2811760.

[33] H. Vu and W. Choi, "A novel dual full-bridge LLC resonant converter for CC and CV charges of batteries for electric vehicles," *IEEE Trans. Ind. Electron.*, vol. 65, no. 3, pp. 2212–2225, Mar. 2018, doi: 10.1109/TIE.2017.2739705.

[34] H. Li et al., "A 6.6kW SiC bidirectional on-board charger," in *Proc. IEEE Appl. Power Electron. Conf. Exposit. (APEC)*, Mar. 2018, pp. 1171–1178, doi: 10.1109/APEC.2018.8341164.

[35] N. Shafiei, M. Ordonez, M. Craciun, C. Botting, and M. Edington, "Burst mode elimination in high-power *LLC* resonant battery charger for electric vehicles," *IEEE Trans. Power Electron.*, vol. 31, no. 2, pp. 1173–1188, Feb. 2016, doi: 10.1109/TPEL.2015.2420573.

[36] I. Lee, "Hybrid PWM-resonant converter for electric vehicle on-board battery chargers," *IEEE Trans. Power Electron.*, vol. 31, no. 5, pp. 3639–3649, May 2016, doi: 10.1109/TPEL.2015.2456635.

[37] H. Haga and F. Kurokawa, "A novel modulation method of the full bridge three-level LLC resonant converter for battery charger of electrical vehicles," in *Proc. IEEE Energy Convers. Congr. Exposit. (ECCE)*, Oct. 2015, pp. 5498–5504, doi: 10.1109/ECCE.2015.7310433.

[38] J. Deng, S. Li, S. Hu, C. Chris Mi, and R. Ma, "Design methodology of LLC resonant converters for electric vehicle battery chargers," *IEEE Trans. Veh. Technol.*, vol. 63, no. 4, pp. 1581–1592, May 2014, doi: 10.1109/TVT.2013.2287379.

[39] K. Colak, E. Asa, M. Bojarski, and D. Czarkowski, "Hybrid control approach of CLL resonant converter for EV battery chargers," in *Proc. IECON 40th Annu. Conf. IEEE Ind. Electron. Soc.*, Oct. 2014, pp. 5041–5046, doi: 10.1109/IECON.2014.7049266.

[40] J.-Y. Lee and H.-J. Chae, "6.6-kW onboard charger design using DCM PFC converter with harmonic modulation technique and two-stage DC/DC converter," *IEEE Trans. Ind. Electron.*, vol. 61, no. 3, pp. 1243–1252, Mar. 2014, doi: 10.1109/TIE.2013.2262749.

[41] N. D. Dao, D. Lee, and Q. D. Phan, "High-efficiency SiC-based isolated three-port DC/DC converters for hybrid charging stations," *IEEE Trans. Power Electron.*, vol. 35, no. 10, pp. 10455–10465, Oct. 2020, doi: 10.1109/TPEL.2020.2975124.

[42] B. Lee, J. Kim, S. Kim, and J. Lee, "A PWM SRT DC/DC converter for 6.6-kW EV onboard charger," *IEEE Trans. Ind. Electron.*, vol. 63, no. 2, pp. 894–902, Feb. 2016, doi: 10.1109/TIE.2015.2480384.

[43] Y. Kim and J. Lee, "Full-bridge+SRT hybrid DC/DC converter for a 6.6-kW EV on-board charger," *IEEE Trans. Veh. Technol.*, vol. 65, no. 6, pp. 4419–4428, Jun. 2016, doi: 10.1109/TVT.2016.2535237.

[44] J. Park, M. Kim, and S. Choi, "Zero-current switching series loaded resonant converter insensitive to resonant component tolerance for battery charger," *IET Power Electron.*, vol. 7, no. 10, pp. 2517–2524, Oct. 2014, doi: 10.1049/iet-pel.2013.0757.

[45] Z. Li, X. Yang, Y. Li, J. Li, B. Zhang, and T. Lei, "Design and implementation of a high-efficiency DC/DC converter for EVs charging basing on LLC resonant topology and silicon-carbide devices," in *Proc. IEEE Int. Power Electron. Appl. Conf. Exposit. (PEAC)*, Nov. 2018, pp. 1–6, doi: 10.1109/PEAC.2018.8590636.

[46] S. A. Arshadi, M. Ordonez, W. Eberle, M. Craciun, and C. Botting, "Three-phase LLC battery charger: Wide regulation and improved light-load operation," *IEEE Trans. Power Electron.*, vol. 36, no. 2, pp. 1519–1531, Feb. 2021, doi: 10.1109/TPEL.2020.3006422.

[47] H. Wang, M. Shang, and D. Shu, "Design considerations of efficiency enhanced LLC PEV charger using reconfigurable transformer," *IEEE Trans. Veh. Technol.*, vol. 68, no. 9, pp. 8642–8651, Sep. 2019, doi: 10.1109/TVT.2019.2930551.

[48] B. Lee, J. Kim, S. Kim, and J. Lee, "An isolated/bidirectional PWM resonant converter for V2G(H) EV on-board charger," *IEEE Trans. Veh. Technol.*, vol. 66, no. 9, pp. 7741–7750, Sep. 2017, doi: 10.1109/TVT.2017.2678532.

[49] Z. Zhang and A. A. Khaligh (2020) Modelling optimisation of dual-control MHz-level CLLC converter with minimised power losses in battery charging applications, *IET Power Electronics*, vol. 13, pp. 1575–1582, doi: 10.1049/iet-pel.2019.1221.

[50] Z. Zhang, C. Liu, M. Wang, Y. Si, Y. Liu, and Q. Lei, "High-efficiency high-power-density CLLC resonant converter with low-stray-capacitance and well-heat-dissipated planar transformer for EV on-board charger," *IEEE Trans. Power Electron.*, vol. 35, no. 10, pp. 10831–10851, Oct. 2020, doi: 10.1109/TPEL.2020.2980313.

[51] A. M. Ammar, K. Ali, and D. J. Rogers, "A bidirectional GaN-based CLLC converter for plug-in electric vehicles on-board chargers," in *Proc. IECON 46th Annu. Conf. IEEE Ind. Electron. Soc.*, Oct. 2020, pp. 1129–1135, doi: 10.1109/IECON43393.2020.9254560.

[52] H.-T. Chang, T.-J. Liang, and W.-C. Yang, "Design and implementation of bidirectional DC–DC CLLLC resonant converter," in *Proc. IEEE Energy Convers. Congr. Exposit. (ECCE)*, Sep. 2018, pp. 2712–2719, doi: 10.1109/ECCE.2018.8557697.

[53] G. Liu, D. Li, J. Q. Zhang, B. Hu, and M. L. Jia, "Bidirectional CLLC resonant DC–DC converter with integrated magnetic for OBCM application," in *Proc. IEEE Int. Conf. Ind. Technol. (ICIT)*, Mar. 2015, pp. 946–951, doi: 10.1109/ICIT.2015.7125219.

[54] H. Wang, S. Dusmez, and A. Khaligh, "Design and analysis of a full-bridge LLC-based PEV charger optimized for wide battery voltage range," *IEEE Trans. Veh. Technol.*, vol. 63, no. 4, pp. 1603–1613, May 2014, doi: 10.1109/TVT.2013.2288772.

[55] G. Liu, Y. Jang, M. M. Jovanovic, and J. Q. Zhang, "Implementation of a 3.3-kW DC–DC converter for EV on-board charger employing the series-resonant converter with reduced-frequency-range control," *IEEE Trans. Power Electron.*, vol. 32, no. 6, pp. 4168–4184, Jun. 2017, doi: 10.1109/TPEL.2016.2598173.

[56] G. Liu, D. Li, Y. Jang, and J. Zhang, "Over 300 kHz GaN device based resonant bidirectional DCDC converter with integrated magnetics," in *Proc. IEEE Appl. Power Electron. Conf. Exposit. (APEC)*, Mar. 2016, pp. 595–600, doi: 10.1109/APEC.2016.7467932.

[57] Y. Jang, M. M. Jovanovic, J. M. Ruiz, M. Kumar, and G. Liu, "Implementation of 3.3-kW GaN-based DC–DC converter for EV on-board charger with series-resonant converter that employs combination of variable-frequency and delay-time control," in *Proc. IEEE Appl. Power Electron. Conf. Exposit. (APEC)*, Mar. 2016, pp. 1292–1299, doi: 10.1109/APEC.2016.7468035.

[58] S.-H. Ryu, D.-H. Kim, M.-J. Kim, J.-S. Kim, and B.-K. Lee, "Adjustable frequency–duty-cycle hybrid control strategy for full-bridge series resonant converters in electric vehicle chargers," *IEEE Trans. Ind. Electron.*, vol. 61, no. 10, pp. 5354–5362, Oct. 2014, doi: 10.1109/TIE.2014.2300036.

[59] W.-Y. Choi, M.-K. Yang, and H.-S. Cho, "High-frequency-link soft-switching PWM DC–DC converter for EV on-board battery chargers," *IEEE Trans. Power Electron.*, vol. 29, no. 8, pp. 4136–4145, Aug. 2014, doi: 10.1109/TPEL.2013.2288364.

[60] J. Min and M. Ordonez, "Bidirectional resonant CLLC charger for wide battery voltage range: Asymmetric parameters methodology," *IEEE Trans. Power Electron.*, vol. 36, no. 6, pp. 6662–6673, Jun. 2021, doi: 10.1109/TPEL.2020.3033982.

[61] H. Li, S. Wang, Z. Zhang, J. Tang, X. Ren, and Q. Chen, "A SiC bidirectional LLC on-board charger," in *Proc. IEEE Appl. Power Electron. Conf. Exposit. (APEC)*, Mar. 2019, pp. 3353–3360, doi: 10.1109/APEC.2019.8722324.

[62] *Electric Vehicle Conductive Charging Systemapart 23: Dc Electric Vehicle Charging Station*, European Standard IEC 61851-23:2014, 2014.

[63] L. Costa, G. Buticchi, and M. Liserre, "A fault-tolerant series-resonant DC–DC converter," *IEEE Trans. Power Electron.*, vol. 32, no. 2, pp. 900–905, Feb. 2017, doi: 10.1109/TPEL.2016.2585668.

[64] F. Grazian, T. B. Soeiro, and P. Bauer, "Inductive power transfer based on variable compensation capacitance to achieve an EV charging profile with constant optimum load," *IEEE J. Emerg. Sel. Topics Power Electron.*, vol. 11, no. 1, pp. 1230–1244, Feb. 2023, doi: 10.1109/JESTPE.2022.3188060.

[65] K. Venkatachalam, C. R. Sullivan, T. Abdallah, and H. Tacca, "Accurate prediction of ferrite core loss with nonsinusoidal waveforms using only Steinmetz parameters," in *Proc. IEEE Workshop Comput. Power Electron.*, Jun. 2002, pp. 36–41, doi: 10.1109/CIPE.2002.1196712.

[66] S. Rivera, S. Kouro, S. Vazquez, S. M. Goetz, R. Lizana, and E. Romero-Cadaval, "Electric vehicle charging infrastructure: From grid to battery," *IEEE Ind. Electron. Mag.*, vol. 15, no. 2, pp. 37–51, Jun. 2021, doi: 10.1109/MIE.2020.3039039.

[67] S. Rivera et al., "Charging infrastructure and grid integration for electromobility," *Proc. IEEE*, vol. 111, no. 4, pp. 371–396, Apr. 2023, doi: 10.1109/JPROC.2022.3216362.

Bram Oude Aarninkhof received the bachelor's degree in mechanical engineering and the master's degree (cum laude) in electrical power engineering from the Delft University of Technology, Delft, The Netherlands, in 2019 and 2021, respectively. He is currently pursuing the Ph.D. degree in power electronics with the University of Twente, Enschede.

He worked as a Power Electronic Engineer at Lightyear, from 2022 to 2023, where he researched new high efficient dc-dc converters for the use in solar electric vehicles. His current research interests include multi objective design modeling of converters, high frequency magnetic design, and high efficiency power electronics for the electrification of the transportation sector.

Dingsihao Lyu (Member, IEEE) received the B.Sc. degree in electrical engineering from the University of Electronic Science and Technology of China (UESTC), Chengdu, China, in 2017, and the M.Sc. degree in electrical power engineering from the Delft University of Technology, Delft, The Netherlands, in 2019. He is currently pursuing the Ph.D. degree in electrical engineering with DC Systems, Energy Conversion, and Storage (DCES) Group, Delft University of Technology, Delft, The Netherlands.

His current research interests include unidirectional /bidirectional dc/dc power electronic converters and multi-objective design of power electronic converters.

Thiago Batista Soeiro (Senior Member, IEEE) received the B.Sc. (Hons.) and M.Sc. degrees in electrical engineering from the Federal University of Santa Catarina, Florianopolis, Brazil, in 2004 and 2007, respectively, and the Ph.D. degree from the Swiss Federal Institute of Technology, Zurich, Switzerland, in 2012.

He was a Visiting Scholar with the Power Electronics and Energy Research Group, Concordia University, Montreal, QC, Canada, and with the Center for Power Electronics Systems, Blacksburg, VA, USA. From 2012 to 2013, he was a Researcher with the Power Electronics Institute, Federal University of Santa Catarina. From October 2013 to April 2018, he was a Senior Scientist with the Corporate Research Center, ABB Switzerland Ltd., Baden-Dattwil, Switzerland. From May 2018 to January 2022, he was with the DC Systems, Energy Conversion and Storage Group, Delft University of Technology, Delft, The Netherlands, as an Associate Professor. Since October 2022, he has been with the Power Management and Distribution Section (TEC-EPM) for the European Space Research and Technology Center, Noordwijk, The Netherlands, and a Full Professor of power electronics with the Power Electronics and EMC Group, University of Twente, Enschede, The Netherlands. His current research interests include advanced high power converters and dc system integration.

Dr. Soeiro was a recipient of the 2013 IEEE Industrial Electronics Society Best Conference Paper Award and the Best Paper Awards in the following IEEE conferences: International Conference on Power Electronics (ECCE Asia 2011), the International Conference on Industrial Technology (ICIT 2013), the Conference on Power Electronics and Applications EPE'15 (ECCE Europe 2015), and the International Conference on Power Electronics and Motion Control 2020 and 2022 (PEMC 2020 and 2022).

Pavol Bauer (Senior Member, IEEE) received the master's degree in electrical engineering from the Technical University of Kosice, Koice, Slovakia, in 1985, and the Ph.D. degree from the Delft University of Technology, Delft, The Netherlands, in 1995.

He is currently a Full Professor with the Department of Electrical Sustainable Energy of Delft University of Technology and the Head of DC Systems, Energy Conversion and Storage Group. He is also a Professor with the Brno University of Technology, Brno, Czech Republic, and a Honorary Professor with Politehnica University Timişoara, Timişoara, Romania. From 2002 to 2003, he was partially with KEMA, DNVGL, Arnhem on different projects related to power electronics applications in power systems. He has worked on many projects for industry concerning wind and wave energy, power electronic applications for power systems, such as Smarttrafo and HVDC systems, projects for smart cities, such as PV charging of electric vehicles, PV and storage integration, contactless charging, and participated in several Leonardo da Vinci, H2020 and Electric Mobility Europe EU Projects as Project partner (ELINA, INETELE, E-Pragmatic, Micact, Trolley 2.0, OSCD, P2P, Progressus) and a Coordinator (PEMCWebLab.com-Edipe, SustEner, Eranet DCMICRO). He authored or coauthored more than 120 journal and 500 conference papers in his field (with H factor Google scholar 40,Web of Science 26). He is the author or coauthor of eight books, holds seven international patents and organized several tutorials at the international conferences. His main research interests include power electronics for charging of electric vehicles and dc grids.

Dr. Bauer is the former Chairman of the Benelux IEEE Joint Industry Applications Society, the Power Electronics and Power Engineering Society chapter, and the Power Electronics and Motion Control (PEMC) council, and a member of the Executive Committee of European Power Electronics Association (EPE) and International Steering Committee at numerous conferences.